

1                   **Cavity-Enhanced Absorption Sensor for Carbon Monoxide**  
2   **in a Rapid Compression Machine**

3   Ehson F. Nasir<sup>1</sup>, Aamir Farooq\*<sup>1</sup>

4           <sup>1</sup> King Abdullah University of Science and Technology, Clean Combustion Research Center, Physical  
5   Sciences and Engineering Division, Thuwal, 23955-6900, Saudi Arabia

6  
7   **Colloquium: Diagnostics**

8   \*Corresponding Author: [aamir.farooq@kaust.edu.sa](mailto:aamir.farooq@kaust.edu.sa)

9   Clean Combustion Research Center

10   King Abdullah University of Science and Technology (KAUST)

11   Thuwal, 23955-6900, Saudi Arabia

12  
13   **Word Count (Method 1):**

15 **Cavity-Enhanced Absorption Sensor for Carbon Monoxide**  
16 **in a Rapid Compression Machine**

17 Ehson F. Nasir<sup>1</sup>, Aamir Farooq\*<sup>1</sup>

18 <sup>1</sup> King Abdullah University of Science and Technology, Clean Combustion Research Center, Physical  
19 Sciences and Engineering Division, Thuwal, 23955-6900, Saudi Arabia

20  
21 **Abstract**

22 A sensor based on cavity-enhanced absorption spectroscopy (CEAS) was implemented for the first time  
23 in a rapid compression machine (RCM) for carbon monoxide concentration measurements. The sensor  
24 consisted of a pulsed quantum cascade laser (QCL) coupled to a low-finesse cavity in the RCM using an  
25 off-axis alignment. The QCL was tuned near 4.89  $\mu\text{m}$  to probe the P(23) ro-vibrational line of CO. The  
26 pulsed mode operation resulted in rapid frequency down-chirp ( $6.52 \text{ cm}^{-1}/\mu\text{s}$ ) within the pulse as well as  
27 a high time resolution (10  $\mu\text{s}$ ). The combination of rapid frequency down-chirp and off-axis cavity  
28 alignment enabled a near complete suppression of the cavity coupling noise. A CEAS gain factor of 133  
29 was demonstrated in experiments, resulting in a much lower noise-equivalent detection limit than a single-  
30 pass arrangement. The sensor thus presents many opportunities for measuring CO formation at low  
31 temperatures and for studying kinetics using dilute reactive environments; one such application is  
32 demonstrated in this work using dilute n-heptane/air mixtures in the RCM. The formation of CO during  
33 first-stage ignition of n-heptane was measured over 802 – 899 K at a nominal pressure of 10 bar. These  
34 conditions correspond to the NTC region of n-heptane and such results provide useful metrics to test and  
35 compare the predictions of low-temperature heat release by different kinetic models.

36 **Keywords:** *Rapid compression machine; Cavity-enhanced absorption spectroscopy; Carbon monoxide;*  
37 *Low-temperature heat release; n-heptane.*

## 38 1. Introduction

39 The auto-ignition behavior of hydrocarbon fuels is determined by chemical processes that are  
40 temperature-specific. For the intermediate temperature range (700 – 900 K), certain classes of  
41 hydrocarbons, such as paraffins, exhibit two stages of heat release during their oxidation, with the first  
42 stage often referred to as low-temperature heat release (LTHR). Several previous works have shown that  
43 LTHR is primarily sensitive to reactions involving fuel radicals and is thus fuel-specific. Consequently,  
44 low-temperature oxidation is more challenging to model than high-temperature chemistry which is  
45 controlled by smaller radical species [1, 2]. Moreover, LTHR can influence overall ignition and this  
46 property can be leveraged to increase knock resistance in SI engines [3] or to control the heat release rate  
47 in HCCI engines [4].

48

49 Rapid compression machines (RCM) have been important tools in studying LTHR and the kinetics of  
50 low-temperature ignition [5]. RCMs offer an operating range of temperatures that cover both the low and  
51 intermediate temperature range (600 – 900 K) as well as high pressures encountered in practical  
52 combustion systems (10 – 40 bar). RCMs also provide much longer test times than shock tubes (5 – 100  
53 ms) and, therefore, ignition delay times, measured using pressure traces in RCMs, are typically used for  
54 validating low-temperature kinetic models. However, ignition delay times provide a global view of the  
55 overall ignition process; time-resolved laser diagnostics can offer a much deeper insight into the kinetics  
56 through measured species concentration and/or temperature profiles.

57

58 Semiconductor lasers, particularly quantum cascade lasers (QCLs) in the mid-infrared wavelength region,  
59 have been successfully used for sensitive, time-resolved species concentration measurements, based on  
60 laser absorption spectroscopy, in transient reactors such as shock tubes [6, 7]. In RCMs, however, limited  
61 studies exist in the literature on applications of semiconductor laser absorption diagnostics. Early

62 applications were demonstrated by Sung and co-workers [8, 9] for measuring H<sub>2</sub>O concentration using a  
63 mid-infrared QCL, though their sensor lacked sufficient time resolution. A previous publication by the  
64 authors of the current work made use of intrapulse absorption with pulsed QCLs for time-resolved  
65 temperature measurements in an RCM [10]. The intrapulse technique offered significant benefits over  
66 previous QCL implementations in terms of both high time resolution and large spectral tuning range. More  
67 recently, Werblinski et al. have demonstrated high time-resolution (50 – 100 μs) measurements of H<sub>2</sub>O  
68 concentration in an RCM using a near-infrared supercontinuum laser source [11, 12].

69

70 Laser absorption measurements are path-averaged in nature and, therefore, work best in homogeneous gas  
71 environments. Reactor configurations for creating ideal constant volume conditions, such as shock tubes  
72 and RCMs, are designed to achieve homogeneous environments in order to reduce sensitivity of chemical  
73 processes to transport phenomena. RCMs attempt to suppress thermal boundary layer mixing with the  
74 core gas via the use of crevices, though thermal gradients can still arise due to first-stage ignition [13] or  
75 due to certain conditions promoting pre-ignition [14]. The use of highly dilute reactive mixtures can  
76 greatly reduce heat release and ensure a homogeneous temperature field is maintained. Such mixtures  
77 require sensors of higher sensitivity than conventional laser absorption diagnostics. One method of  
78 increasing the sensitivity of laser absorption spectroscopy has been to increase the path length of  
79 measurement via cavity enhancement. A specific cavity technique, known as cavity-enhanced absorption  
80 spectroscopy (CEAS), has been successfully demonstrated by Hanson and co-workers in recent shock  
81 tube studies for several species [15, 16].

82

83 In this work, we have demonstrated the use of a sensor based on CEAS for measuring CO concentration  
84 in the RCM. The CEAS sensor enabled us to achieve a much lower detection limit than would have been  
85 possible with a conventional single-pass technique using the same absorption transition. The improved

86 sensitivity allowed for the investigation of first-stage ignition kinetics of n-heptane using diluted reactant  
87 mixtures. The dilution of fuel suppressed first-stage heat release and thus the adiabatic core assumption  
88 remained valid after the first-stage ignition. This is the first reported application of the CEAS technique  
89 in an RCM and the results highlight the potential of the technique in other RCM experiments involving  
90 highly dilute reactant mixtures and for measuring radicals / trace species.

91

## 92 2. CEAS principles

93 For conventional laser absorption spectroscopy, absorption of spectrally narrow light is related to  
94 gas properties *via* the Beer-Lambert relation:

$$95 \ln(I_0/I_t) = A_{SP} = (SPXL\Phi_\nu) \quad (1)$$

96 In this relation,  $A_{SP}$  is the absorbance for a single-pass arrangement which is directly proportional to the  
97 mole fraction  $X$  of the absorbing species. The goal of any absorption experiment is to maximize the  
98 absorption signal ( $I_0/I_t$ ) for a given  $X$ . The line-strength  $S$  and line-shape function  $\Phi_\nu$  are specific to a  
99 particular molecular absorption transition and, therefore, for a given absorption transition and  
100 experimental gas conditions ( $T, P, X$ ), the only possibility for increasing the absorption signal is to increase  
101 the path length  $L$ . An optical cavity, made of two parallel concave mirrors, accomplishes this through  
102 multiple reflections. In such a cavity, the absorbance will be defined as  $A_{CEAS}$ , where:

$$103 \ln(I_0/I_t) = A_{CEAS} = \ln(1 + GA_{SP}) \quad (2)$$

104 provided that  $A_{SP} \ll 1$  [16, 17]. The term  $G$  refers to the gain factor of the cavity and is related to the  
105 reflectivity  $R$  of the mirrors through the following relation:

$$106 G = 1/(1 - R) \quad (3)$$

107 While the cavity gain only depends on the mirror reflectivity, the signal-to-noise ratio (SNR) is also  
108 dependent on how well the laser beam couples with the resonant modes of the cavity. For an optical cavity,  
109 the free spectral range (FSR) determines the spectral spacing between resonant cavity modes:

110 
$$\text{FSR} = 1 / 2nL \text{ (in cm}^{-1} \text{ units)} \quad (4)$$

111 where  $n$  is the refractive index of the medium. Effective coupling requires matching the laser emission  
112 mode with at least one cavity mode. If the laser line-width is narrower than the cavity FSR, spurious mode-  
113 matching can be achieved through off-axis alignment, as described by Engel et al. [18]. Off-axis alignment  
114 results in a Lissajous spot pattern on the cavity mirrors [19] and the effective cavity FSR is reduced by  
115 the number of non-overlapping spots, thus increasing the likelihood of resonance between cavity modes  
116 and a narrow line-width laser. A necessary requirement for off-axis alignment is to use a cavity made of  
117 concave mirrors such that the cavity length is much smaller than the focal length of the mirrors.  
118 Additionally, Sun et al. [16] showed that the cavity noise can be suppressed further by a rapid scan of the  
119 laser frequency, further increasing the likelihood of spurious mode-matching.

120

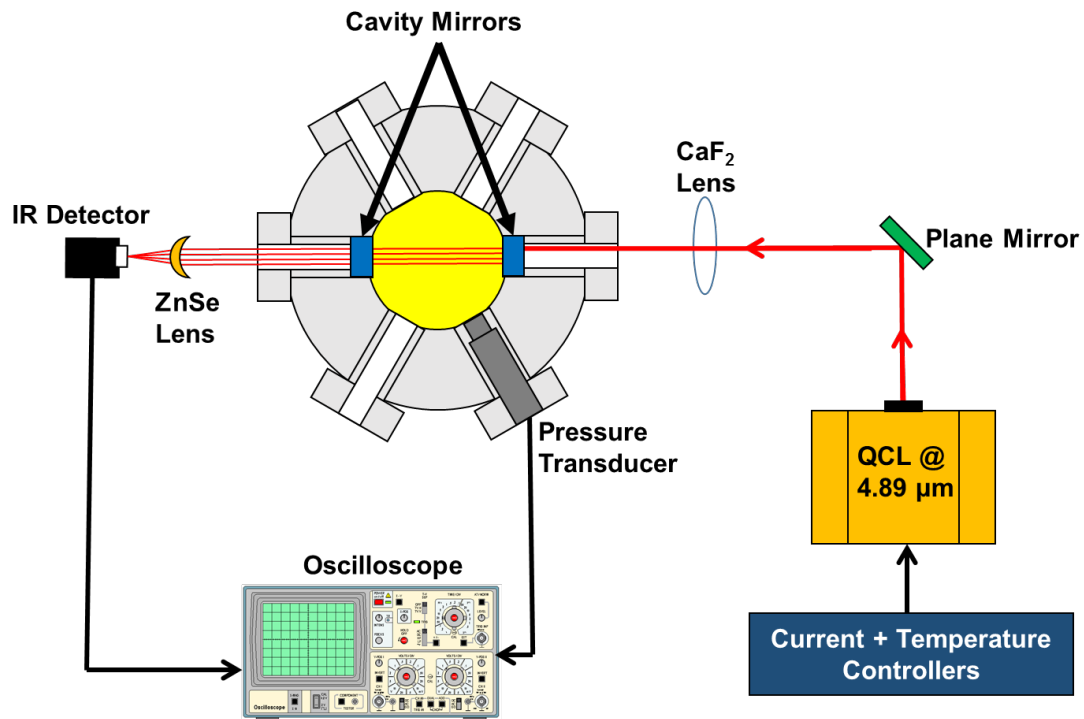
### 121 **3. Sensor implementation**

122 The measurement target of the CEAS sensor in this work is carbon monoxide due its relevance to  
123 LTHR, as described by Tekawade et al. [20]. A pulsed distributed feedback (DFB) QCL system sourced  
124 from Alpes Lasers, was used to probe the P(23) ro-vibrational transition of CO near  $2046.28 \text{ cm}^{-1}$  ( $4.887$   
125  $\mu\text{m}$ ). A detailed description of the laser system can be found in a previous publication [10]. Relevant  
126 spectroscopic parameters needed to convert the single-pass absorbance to mole fraction were taken from  
127 the HITRAN 2016 database [21].

128

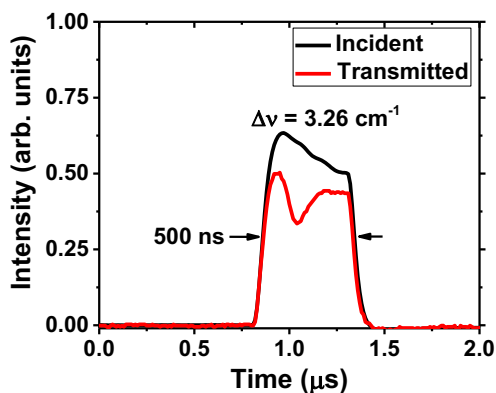
129 In this work, the CEAS technique was implemented on the KAUST RCM facility. While relevant details  
130 are mentioned here, further information about the facility can be found elsewhere [10, 22, 23]. The optical  
131 cavity was formed by installing highly reflective concave mirrors (sourced from Rocky Mountain  
132 Instrument Co.) on the centrally located ports of the RCM combustion chamber. The RCM has an internal  
133 diameter of  $5.08 \text{ cm}$ , which serves as the single-pass path length, resulting in a cavity FSR of  $0.0984 \text{ cm}^{-1}$

134 <sup>1</sup>. The cavity mirrors had a manufacturer-specified reflectivity of  $99.5 \pm 0.2\%$  at  $4.887 \mu\text{m}$  and a radius  
135 of curvature of  $-1 \text{ m}$ . The QCL was aligned in an off-axis arrangement to produce a small ellipsoidal spot  
136 pattern on the cavity mirrors. The light was collected on the receiving end using an aspheric ZnSe lens  
137 (focal length  $12.7 \text{ mm}$ ), as shown in Fig. 1, and focused on a high bandwidth ( $500 \text{ MHz}$ ) HgCdTe detector  
138 from Vigo System ( $1 \text{ mm}^2$  active area). The detector signal was acquired by an oscilloscope at  $100 \text{ MHz}$   
139 sampling rate.



140  
141 Fig. 1. Schematic of the laser sensor aligned through the cross-section of the RCM combustion chamber.  
142

143 The QCL was operated in pulsed mode with a pulse repetition frequency of  $100 \text{ kHz}$  and a pulse duration  
144 of  $500 \text{ ns}$ , resulting in an effective time resolution of  $10 \mu\text{s}$ . Upon examination with a Germanium etalon,  
145 the intrapulse spectral tuning range was found to be  $3.26 \text{ cm}^{-1}$ . The average frequency scan rate of  $6.52$   
146  $\text{cm}^{-1}/\mu\text{s}$  in this case is two orders of magnitude higher than that reported by Sun et al. [16] using injection  
147 current scanning with a cw-QCL. The extremely rapid scan rate combined with an off-axis alignment  
148 resulted in an almost complete suppression of cavity coupling noise, as illustrated in Fig. 2.



149

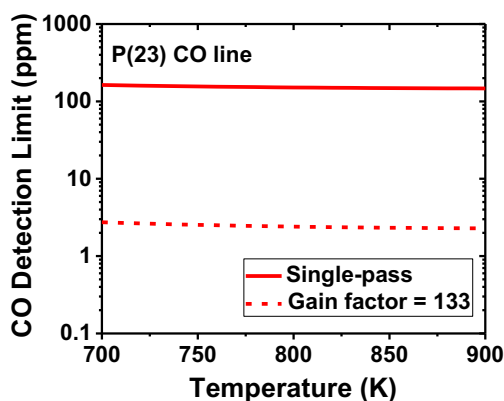
150 Fig. 2. Representative laser intensity signal showing absorption by CO in the transmitted trace. Conditions: 100  
 151 ppm CO/N<sub>2</sub>, 796 K, 10.5 bar.

152

153 The uncertainty specified by the manufacturer on the mirror reflectivity ( $\pm 0.2\%$ ) can translate into a large  
 154 uncertainty in the gain factor (143 – 333). Significant deviations from the manufacturer-specified  
 155 reflectivity can occur [17]. Therefore, to determine the actual mirror reflectivity and to reduce the  
 156 uncertainty, the CEAS sensor was tested against known mixtures of CO/N<sub>2</sub> at high pressures ( $> 5$  bar) for  
 157 both ambient temperature as well as higher temperature conditions in the RCM. Using the measured peak  
 158 CEAS absorbance ( $A_{\text{CEAS}}$ ) and the calculated peak single-pass absorbance ( $A_{\text{SP}}$ ) using HITRAN  
 159 parameters, the reflectivity can be ascertained through Eqs. 2 and 3. The mirror reflectivity from these  
 160 experiments was found to be  $99.25 \pm 0.04\%$ , which translates to a gain factor of  $133 \pm 8$ . The gain was  
 161 not found to be significantly affected by the compression process despite low-frequency intensity  
 162 fluctuations in the laser signal due to mechanical vibrations. Measurement of mirror reflectivity results in  
 163 a factor of five reduction in the uncertainty compared to the manufacturer specification. The gain factor  
 164 can then be used to establish a new detection limit for CO measurements based on a fixed absorbance.  
 165 Figure 3 shows a comparison between the detection limit offered by a single-pass arrangement and that  
 166 provided by a CEAS arrangement for typical RCM operating conditions (10 bar, 700 – 900 K). It is clear  
 167 that the CEAS technique provides a substantial improvement in detection limit and hence SNR. As an



168 example, at 800 K the CEAS detection limit (2.4 ppm) is 63 times lower than the single-pass detection  
169 limit (151 ppm).



170

171 Fig. 3. Comparison of detection limit for single-pass and CEAS (with gain factor of 133). Calculated with  
172 HITRAN parameters [21] at 10 bar total pressure and assuming minimum-detectable-absorbance of 0.01.

173

#### 174 4. RCM experiments with n-heptane

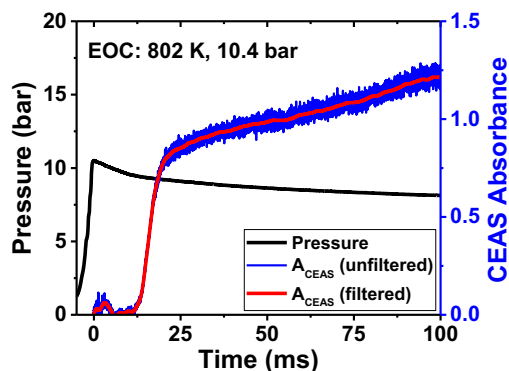
175 The CEAS sensor was applied to RCM experiments involving the oxidation of lean n-heptane/air  
176 mixtures. n-Heptane is a highly reactive fuel, defined to have zero octane number, and therefore ignition  
177 delay studies of n-heptane in an RCM require tailored experimental conditions such that the ignition delay  
178 time is in a measurable range. For RCM experiments on fuels depicting two-stage ignition behavior, it is  
179 preferable to have at least a 5 ms delay between the end-of-compression (EOC) and first-stage ignition to  
180 avoid significant chemical activity during the compression phase. Moreover, Mittal et al. [13] showed that  
181 in the event of significant LTHR, the increasingly energetic core gas could compress the cold boundary  
182 layer and expand into the crevice region, resulting in a lower post-ignition temperature than predicted  
183 using the adiabatic core assumption. This was recently confirmed through *in situ* laser-based temperature  
184 measurements in the KAUST RCM [10]. In light of these considerations, experimental conditions were  
185 chosen such that LTHR would be significantly reduced and first-stage ignition delay would be lengthened  
186 beyond 5 ms. A mixture of n-heptane, oxygen and nitrogen at equivalence ratio of 0.5 was used, where

187 the n-heptane mole fraction was kept at 0.2% as opposed to nearly 1% for an undiluted mixture. A  
188 temperature range of  $\sim 800 - 900$  K was covered at a nominal pressure of 10 bar; these conditions  
189 correspond to the NTC region of n-heptane.

190 Figure 4 shows experimental results for a specific n-heptane oxidation case at 802 K and 10.4 bar. The  
191 large rise in CO absorbance near 13 ms marks first-stage ignition, while second-stage ignition is not  
192 observed for this highly dilute reactive mixture. The measured pressure trace in Fig. 4 provides no  
193 indication of a pressure rise associated with LTHR near 13 ms (a comparison with non-reactive pressure  
194 profiles is provided in Figs. S1 and S2), in contrast with our previous work with undiluted n-pentane  
195 mixtures in which the onset of 1<sup>st</sup> stage ignition was clearly discerned from the pressure rise [10]. Thus,  
196 in these diluted n-heptane experiments, heat release (LTHR) at the onset of first-stage ignition is negligibly  
197 small and the gas mixture can be considered isentropic up to, and beyond, EOC. Based on the adiabatic  
198 core assumption [5], the temperature in RCM experiments is normally inferred from the measured pressure  
199 trace by using the isentropic relation:

$$200 \quad \int_{T_I}^T \frac{\gamma}{\gamma-1} \frac{dT}{T} = \ln \left( \frac{P}{P_I} \right) \quad (5)$$

201 The subscript  $I$  in this relation refers to the initial conditions prior to compression. Given the dilute fuel  
202 concentration in our case as well as the observation that the mixture does not reach 2<sup>nd</sup> stage ignition (an  
203 indication that most of the initial fuel remains unconsumed), for the purpose of calculating thermodynamic  
204 parameters for Eq. 5, the initial reactant mixture composition (dominated by nitrogen) is used for the  
205 temperature profile beyond EOC. For experiments in this work, temperature profile calculated from Eq. 5  
206 was used for spectroscopic parameters in the Beer-Lambert relation.



207

208 Fig. 4. Representative measured CEAS absorbance and pressure traces. EOC conditions: 802 K, 10.4 bar. Initial  
 209 composition: 0.2% n-heptane/4.4% O<sub>2</sub>/95.4% N<sub>2</sub> ( $\phi = 0.5$ ).

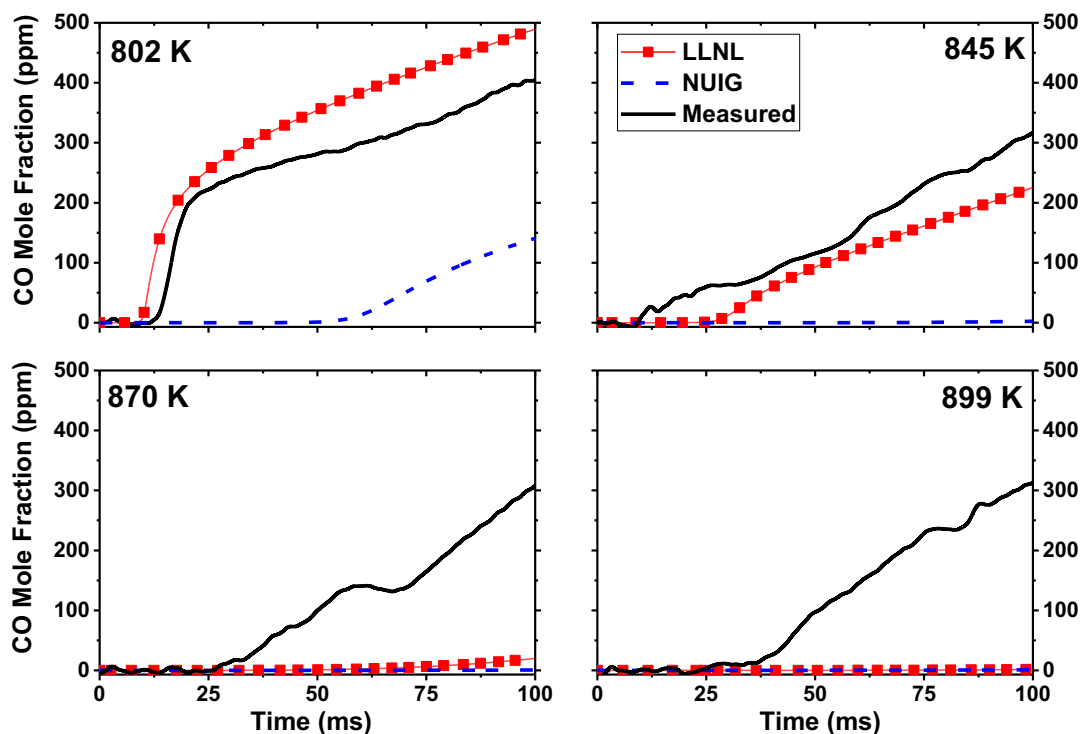
210

211 For the purpose of determining CO mole fraction, only the peak CEAS absorbance was used for each laser  
 212 pulse. Using the measured CEAS absorbance and gain factor, the single pass absorbance can be  
 213 determined from Eq. 2, which in turn is used in Eq. 1 for computing the CO mole fraction. The unfiltered  
 214 CEAS absorbance plot in Fig. 4 exhibits high-frequency noise that can be attributed to a combination of  
 215 sampling bit noise and pulse-to-pulse intensity variation. The filtered trace in Fig. 4 is a result of applying  
 216 a 2 kHz low-pass filter during post-processing. A small deviation in the laser signal (beam steering) occurs  
 217 near EOC due to the effect of mechanical vibration on the laser alignment. The CEAS absorbance plot  
 218 presented here has been corrected for a small background (interference) absorption by n-heptane. This  
 219 background was determined by the average absorbance between EOC and first-stage ignition. The  
 220 background was found to be similar for various conditions and since complete fuel conversion is not  
 221 expected to occur at such dilute conditions, the background can be assumed to remain nearly constant  
 222 during the experiment.

223

224 Figure 5 shows measured carbon monoxide mole fraction traces, calculated from the filtered CEAS  
 225 absorbance profiles, at four different EOC temperatures. The rise of CO formation in all cases denotes the  
 226 onset of LTHR. Since these conditions lie in the NTC region of n-heptane, the first-stage ignition delay is

227 expected to increase with temperature, which is substantiated by an observed decrease in measured CO  
228 formation rate with increasing temperature. Despite the potential for beam steering effects from flow or  
229 mechanical perturbations over a time window of  $\sim 100$  ms, the CEAS sensor successfully captures time-  
230 resolved, quantitative species information that can serve as validation target for kinetic models.



231

232 Fig. 5. Measured CO mole fraction overlaid with simulation results from LLNL and NUIG n-heptane  
233 mechanisms. Initial composition: 0.2% n-heptane/4.4% O<sub>2</sub>/95.4% N<sub>2</sub>. Nominal EOC pressure is 10 bar.

234

235 Included in Fig. 5 are simulation results obtained using the n-heptane mechanisms developed at LLNL  
236 [24] and NUI Galway [25] (a further comparison of simulated temperature profiles is provided in Fig. S3).  
237 The simulations were performed in Chemkin-Pro software package using isentropic volume profiles to  
238 model the compression phase as well as post-compression heat loss. These volume profiles were generated  
239 from pressure traces measured in non-reactive experiments carried out at EOC conditions similar to the  
240 respective reactive experiments. Although both LLNL and NUIG models show an increasing trend for  
241 first-stage ignition delay, the increase in ignition delay time with respect to temperature is significantly

242 higher than that observed in experiments. The LLNL model is in approximate agreement with the  
243 experimental data at 802 and 845 K but deviates significantly at higher temperatures. By contrast, the  
244 NUIG model predicts much higher ignition delay (by factor of 4) at 802 K than the experiment, while for  
245 higher temperatures the predicted rise in CO formation is no longer within the 100 ms window. In a  
246 previous study, a comparison of predictions of total ignition delay between the NUIG and LLNL models  
247 showed that, for undiluted conditions, the NUIG model does indeed predict longer ignition delays (refer  
248 to Fig. 8a in [25]). However, the magnitude of the discrepancy between the LLNL and NUIG models  
249 (factor of 1.5) was found to be significantly less than what has been observed here for diluted conditions.  
250 The controlling factors for ignition delay times at these conditions are the addition of O<sub>2</sub> to the fuel alkyl  
251 radical as well as the decomposition or isomerization of the resultant alkylperoxy radical. Due to the  
252 dependence of the overall reactivity on the alkyl radical, fuel concentration plays a significant role in  
253 determining the timing of LTHR. Diluted fuel/air mixtures thus greatly exaggerate differences in ignition  
254 delay between the two kinetic models and allow for a much clearer comparison with experimental data.

255

## 256 **5. Measurement uncertainty**

257 Equations 1 and 2, which are used to compute CO mole fraction, include factors that contribute to  
258 the overall uncertainty in the measured mole fraction. These factors are: the gain factor  $G$ , line-strength  $S$   
259 and the line-shape function  $\Phi_v$ . The latter two are determined from the HITRAN database and are  
260 temperature-dependent. Thus the uncertainties in the HITRAN values as well as the uncertainty in  
261 temperature need to be propagated to the mole fraction uncertainty. The error codes within the HITRAN  
262 data files provide uncertainties for line-strength, as well as for air-broadening coefficient and the  
263 temperature exponent of broadening which are used to calculate the line-shape function.

264

265 As mentioned earlier, tests with CO/N<sub>2</sub> mixtures in the RCM yielded an uncertainty of 6.02% in the gain  
266 factor ( $G$ ). This uncertainty resulted from measurement errors due to pulse-to-pulse intensity variation as  
267 well as mechanical perturbations affecting the laser signal. The RCM used in this work has creviced piston  
268 heads to prevent mixing of the thermal boundary with the core gas, thus establishing a homogeneous  
269 temperature field at the end of compression phase. Nevertheless, after EOC, the thermal boundary layer  
270 is expected to grow due to heat loss, especially in the measurement time window of 100 ms used in this  
271 work. Mittal et al. [26] showed that the influence of the boundary layer on the core gas is inversely related  
272 to the piston stroke length. For an EOC pressure of 10 bar, their simulation results showed a 1% change  
273 in average core gas temperature for a piston stroke length of 17.78 cm. For our RCM facility, the stroke  
274 length is 16.9 cm [10] and, therefore, the result from Mittal et al. can serve as a reasonable estimate for  
275 the uncertainty in temperature. Moreover, the measured laser absorption is a sum of absorption in the core  
276 gas as well as the absorption in the boundary layer. Assuming that the boundary layer thickness increases  
277 with thermal diffusivity and time ( $\delta \sim \sqrt{\alpha t}$ ), the thickness is expected to be about 15% of the total path  
278 length at 100 ms. The effective temperature in the boundary layer is assumed to be an average of the core  
279 gas and wall temperature, which, coupled with the boundary layer thickness, translates to an uncertainty  
280 of 4.05% in the absorbance. This represents an upper limit for the uncertainty estimate since the boundary  
281 layer thickness will be much smaller at the early (< 100 ms) measurement times.

282

283 Each of the aforementioned parameters was perturbed to its uncertainty limits and the resultant effect on  
284 the value of the CO mole fraction was calculated. The effect from each parameter is shown in Table 1.  
285 The total uncertainty in the CO mole fraction is calculated as the root-sum-square of the individual  
286 contributions, and is found to be 8.51% at a nominal condition of 850 K and 10 bar. It may be seen in Fig.  
287 3 that for the temperature range of interest in RCMs, i.e. 700 – 900 K, the minimum detection limit of CO  
288 for the P(23) transition has very weak temperature dependence. Thus, the CEAS measurements are

289 expected to be largely unaffected by any temperature changes in this temperature range. The uncertainty  
290 in measurements due to pressure would increase significantly at lower pressures as the laser line-width  
291 becomes comparable with the molecular collisional width. Thus, as in the previous study [10], the  
292 diagnostic was applied to high-pressure (10 bar) measurements to avoid this issue. At higher pressures (>  
293 20 bar), the collisional broadening would become large enough to cause interference of the P(23) line with  
294 other CO as well as non-CO lines in spectral proximity.

295 Table 1. Uncertainty contributions to CO mole fraction measurements. Conditions: 850 K, 10 bar,  $A_{CEAS} = 0.5$ .

<b>Parameter</b>	<b>% Uncertainty</b>	<b>% Effect on <math>X_{CO}</math></b>
Temperature	1.00	0.25
Boundary layer absorption	4.05	5.16
Gain Factor	6.02	6.06
Line-strength	1.00	1.01
Broadening coefficient	1.50	1.47
Temperature exponent	3.50	2.43
<b>Total Uncertainty in CO mole fraction</b>		<b>8.51%</b>

296

## 297 6. Conclusions

298 A highly sensitive CEAS (cavity-enhanced absorption spectroscopy) sensor for quantitative and  
299 sensitive measurements of carbon monoxide has been demonstrated for investigating LTHR (low-  
300 temperature heat release) of dilute n-heptane mixtures in a rapid compression machine. The sensor was  
301 based on a pulsed QCL which provided excellent suppression of cavity coupling noise through rapid  
302 intrapulse frequency tuning. A significant reduction in the minimum detection limit for CO was achieved  
303 and this holds great potential for applications in ignition studies that use diluted fuel/air mixtures. The

304 effect of dilution was shown to minimize thermal effects on the kinetic behavior as well as illuminate  
305 differences between experiments and modelling results more clearly. Improved sensitivity in species  
306 concentration measurements, as achieved with CEAS, would prove useful in detecting trace intermediate  
307 combustion species formed at low temperature conditions such as H<sub>2</sub>O<sub>2</sub>, HO<sub>2</sub> and CH<sub>2</sub>O. New sensing  
308 strategies, such as the one demonstrated here, are likely to become important in expanding the  
309 measurement capabilities of RCM facilities.

310

### 311 **Acknowledgments**

312 Research reported in this publication was supported by funding from the Office of Sponsored Research at  
313 King Abdullah University of Science and Technology (KAUST).

314

### 315 **References**

- 316 [1] C.K. Westbrook, Proc. Combust. Inst., 28 (2000) 1563-1577.
- 317 [2] P. Zhang, W. Ji, T. He, *et al.*, Combust. Flame, 167 (2016) 14-23.
- 318 [3] D. Vuilleumier, M. Sjöberg, SAE International Journal of Engines, 10 (2017) 938-950.
- 319 [4] Y. Yang, J.E. Dec, N. Dronniou, M. Sjöberg, Proc. Combust. Inst., 33 (2011) 3047-3055.
- 320 [5] C.J. Sung, H.J. Curran, Prog. Energy Combust. Sci., 44 (2014) 1-18.
- 321 [6] R.K. Hanson, Proc. Combust. Inst., 33 (2011) 1-40.
- 322 [7] C.S. Goldenstein, R.M. Spearrin, J.B. Jeffries, R.K. Hanson, Prog. Energy Combust. Sci., 60 (2017)  
323 132-176.
- 324 [8] A.K. Das, M. Uddi, C.-J. Sung, Combust. Flame, 159 (2012) 3493-3501.
- 325 [9] M. Uddi, A.K. Das, C.-J. Sung, Appl. Opt., 51 (2012) 5464-5476.
- 326 [10] E.F. Nasir, A. Farooq, Proc. Combust. Inst., 36 (2017) 4453-4460.
- 327 [11] T. Werblinski, S. Kleindienst, R. Engelbrecht, L. Zigan, S. Will, Appl. Opt., 55 (2016) 4564-4574.



- 328 [12] T. Werblinski, P. Fendt, L. Zigan, S. Will, *Appl. Opt.*, 56 (2017) 4443-4453.
- 329 [13] G. Mittal, M.P. Raju, C.-J. Sung, *Combust. Flame*, 157 (2010) 1316-1324.
- 330 [14] A.B. Mansfield, M.S. Wooldridge, *Combust. Flame*, 161 (2014) 2242-2251.
- 331 [15] K. Sun, S. Wang, R. Sur, *et al.*, *Opt. Express*, 22 (2014) 9291-9300.
- 332 [16] K. Sun, S. Wang, R. Sur, *et al.*, *Opt. Express*, 22 (2014) 24559-24565.
- 333 [17] A.B.S. Alquaity, U. Kc, A. Popov, A. Farooq, *Appl. Phys. B*, 123 (2017) 280.
- 334 [18] G.S. Engel, W.S. Drisdell, F.N. Keutsch, E.J. Moyer, J.G. Anderson, *Appl. Opt.*, 45 (2006) 9221-  
335 9229.
- 336 [19] J.B. Paul, L. Lapson, J.G. Anderson, *Appl. Opt.*, 40 (2001) 4904-4910.
- 337 [20] A. Tekawade, G. Kosiba, M.A. Oehlschlaeger, *Combust. Flame*, 173 (2016) 402-410.
- 338 [21] I.E. Gordon, L.S. Rothman, C. Hill, *et al.*, *J. Quant. Spectrosc. Radiat. Transfer*, 203 (2017) 3-69.
- 339 [22] T. Javed, E.F. Nasir, A. Ahmed, *et al.*, *Proc. Combust. Inst.*, 36 (2017) 315-322.
- 340 [23] N. Atef, G. Kukkadapu, S.Y. Mohamed, *et al.*, *Combust. Flame*, 178 (2017) 111-134.
- 341 [24] M. Mehl, W.J. Pitz, C.K. Westbrook, H.J. Curran, *Proc. Combust. Inst.*, 33 (2011) 193-200.
- 342 [25] K. Zhang, C. Banyon, J. Bugler, *et al.*, *Combust. Flame*, 172 (2016) 116-135.
- 343 [26] G. Mittal, M.P. Raju, C.-J. Sung, *Fuel*, 94 (2012) 409-417.

344

345

346

347

348

349

350 **List of Figure and Table Captions**

351 **Figure 1.** Schematic of the laser sensor aligned through the cross-section of the RCM combustion  
352 chamber.

353 **Figure 2.** Representative laser intensity signal showing absorption by CO in the transmitted trace.  
354 Conditions: 100 ppm CO/N<sub>2</sub>, 796 K, 10.5 bar.

355 **Figure 3.** Comparison of detection limit for single-pass and CEAS (with gain factor of 133). Calculated  
356 with HITRAN parameters [21] at 10 bar total pressure and assuming minimum-detectable-absorbance of  
357 0.01.

358 **Figure 4.** Representative measured CEAS absorbance and pressure traces. EOC conditions: 802 K, 10.4  
359 bar. Initial composition: 0.2% n-heptane/4.4% O<sub>2</sub>/95.4% N<sub>2</sub> ( $\phi = 0.5$ ).

360 **Figure 5.** Measured CO mole fraction overlaid with simulation results from LLNL and NUIG n-heptane  
361 mechanisms. Initial composition: 0.2% n-heptane/4.4% O<sub>2</sub>/95.4% N<sub>2</sub>. Nominal EOC pressure is 10 bar.

362 **Table 1.** Uncertainty contributions to CO mole fraction measurements. Conditions: 850 K, 10 bar,  $A_{\text{CEAS}}$   
363 = 0.5.